

Neuronal identification of signal periodicity by balanced inhibition

Moritz Bürck · J. Leo van Hemmen

Received: 4 August 2008 / Accepted: 11 March 2009 / Published online: 7 April 2009
© Springer-Verlag 2009

Abstract Many animals, including men, use periodicity information, e.g., amplitude modulations of acoustic stimuli, as a vital cue to auditory object formation. The underlying neuronal mechanisms, however, still remain a matter of debate. Here, we mathematically analyze a model for periodicity identification that relies on the interplay of excitation and delayed inhibition. Our analytical results show how the maximal response of such a system varies systematically with the time constants of excitation and inhibition. The model reliably identifies signal periodicity in the range from about ten to several hundred Hertz. Importantly, the model relies on biologically plausible parameters only. It works best for excitatory and inhibitory neuronal couplings of equal strength, the so-called ‘balanced inhibition’. We show how balanced inhibition can serve to identify low-frequency signal periodicity and how variation of a single parameter, the inhibitory time constant, can tune the system to different frequencies.

Keywords Periodicity detection · Auditory signal processing · Neuronal modeling · Balanced inhibition

1 Introduction

Neuronal processing of acoustic signal periodicity is important for, e.g., hunting and communication and thus survival

in the natural world. Naturally occurring vibrations usually carry information about their source by frequency content and temporal structure, i.e., fluctuations of the frequency content often called amplitude modulations (Langner 1992). The frequency content can be identified by, for example, the cochlea. Some animals, however, such as spiders, the clawed frog or surface feeding fish, can detect and distinguish the frequency of vibratory signals (Bleckmann and Barth 1984; Elepfandt 1984; Käse and Bleckmann 1987) in spite of the fact that their vibration-sensitive organs do not display frequency-specificity (Barth 1998; Coombs et al. 1989; Kalmijn 1988). On the other hand, even mammals that employ a cochlea cannot identify the temporal structure, i.e., amplitude modulations, by means of this organ. Nevertheless amplitude modulations are vital to speech recognition (Shannon et al. 1995), identification of acoustic events (‘cocktail party effect’) (Bregman 1990; Cherry 1953; Yost 1994), and the perception of pitch (Bendor and Wang 2005; Joris et al. 2004). Even more so, typical natural signals in general are a superposition of comodulated frequencies (Nelken et al. 1999). Thus, signal periodicity needs to be processed, or, better, identified *neuronally*. Here we face the question of how to do so.

‘Balanced inhibition’ (BI) denotes inhibitory input of approximately the same strength as the excitatory input. It has been observed at several locations and under various conditions, ranging from cat visual cortex (Anderson et al. 2000; Monier et al. 2003) to the cochlear nucleus in rats (Paolini et al. 2005), and in ongoing as well as sensory-evoked neuronal activity (Okun and Lampl 2008). A number of possible functions have been proposed for BI, but its actual purpose is still a matter of debate. In cat visual cortex it may be important for orientation and direction selectivity of synaptic inputs (Anderson et al. 2000; Monier et al. 2003). In cat auditory cortex, BI is associated with the envelope of

M. Bürck (✉) · J. L. van Hemmen
Physik Department T35, Technische Universität München,
85748 Garching bei München, Germany
e-mail: mbuerck@ph.tum.de

M. Bürck · J. L. van Hemmen
Bernstein Center for Computational Neuroscience,
Munich, Germany

a noise signal if this signal is attended to (Las et al. 2005). Furthermore, it appears to play a role in the processing of frequency modulated tones (Zhang et al. 2003). It has been ruled out to be important to frequency tuning or gain control but has been proposed (Wehr and Zador 2003) to account for enhancing temporal precision and regulating random background activity. In rat cochlear nucleus, BI modulates the chopping frequency in chopper neurons and influences spike firing regularity (Paolini et al. 2005). Rat whisker deflections cause a sequence of excitation and balanced inhibition that is supposed to create a short time window for spikes, like a gate or a filter (Highley and Contreras 2006). The function of this ‘spike window’, however, remains unknown. In the following, we will see that such filtering property, i.e., a neuronal band-pass filter, is indeed a consequence of balanced inhibitory input to a neuron.

How does one identify periodicity in neuronal activity? It is known that neurons selectively responding to specific modulation frequencies exist (Joris et al. 2004; Schreiner and Langner 1988; Speck-Hergenröder and Barth 1987). But how can such a selectivity, a neuronal band-pass characteristic, be explained? A possible solution is to generate the band-pass response in the neurons themselves via membrane dynamics. Here, the spike-generating mechanism may induce oscillations of the membrane potential that follow a spike and thus enhance the firing at certain instants of time after the first spike (Izhikevich 2001). Alternatively, inhibitory input can cause such an oscillation of the membrane potential, the so-called ‘post-inhibitory rebound’ (Large and Crawford 2002). On the level of neuronal circuitry a band-pass characteristic can be realized by excitatory–excitatory interaction or excitatory–inhibitory interaction. The excitatory–excitatory interaction basically works like a coincidence detector where two spikes can only evoke neuronal activity if they arrive at a neuron simultaneously. In other words, if they arrive in phase. The timing of the spikes can either arise from delays (Friedel et al. 2007; Licklider 1951), which gives the neuronal analogon to autocorrelation, or from ‘chopping’ neurons (Meddis and O’Mard 2006), neurons that produce a series of well-timed spikes. Similarly, a band-pass characteristic arises if a single excitatory spike strong enough to evoke neuronal activity is combined with delayed inhibitory spike that arrives in anti-phase to the excitatory input (Grothe 1994). Furthermore, band-pass characteristics within the excitatory–inhibitory setup can also arise from different time constants for excitation and inhibition (Nelson and Carney 2004). This is what we will study in the following.

Similar to the SFIE (Same Frequency Inhibition and Excitation) model proposed by Nelson and Carney (2004) our approach is based on a band-pass characteristic arising from different time constants for excitatory and inhibitory postsynaptic potential (PSP). This is possible because every synapse is a low-pass filter with the ‘cut-off’ frequency

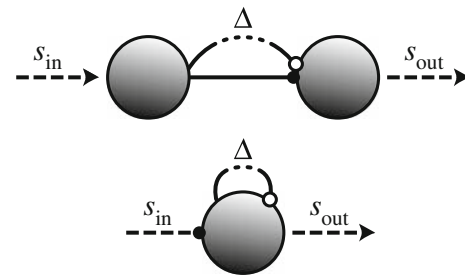


Fig. 1 The two possible ways of extracting frequency or timing information neuronally from a signal using excitatory (closed circles) and inhibitory synapses (open circles). The first method (upper panel) uses a feedforward network, and is called *feedforward model*. The input neuron, driven by a continuous input function s_{in} , sends spikes to the output neuron via a direct excitatory and a *delayed* inhibitory connection, possibly realized by one or more interneurons. Depending on excitatory and inhibitory time constants, certain temporal correlations in the input signal lead to an augmented firing probability for the output neuron. The second method (lower panel) is based on the same idea, but uses an inhibitory recurrent loop with time delay Δ , again possibly realized by one or more interneurons. This we call the *recurrent model*. The neuron is driven again by s_{in} , this time via an excitatory synapse. If the neuron emits a spike at time $t = t_0$, its firing probability is reduced at time $t = t_0 + \Delta$ because of inhibitory feedback. Depending on excitatory and inhibitory time constants, a certain signal periodicity leads to a higher number of spikes in the output signal s_{out}

determined by the neuronal time constant τ of the PSP. A larger τ will lead to a lower ‘cut-off’ frequency of the synapse. According to this consideration, the combination of an excitatory synapse with small τ_{exc} and an inhibitory synapse with large τ_{inh} projecting to the same population of neurons will lead to a bandpass characteristic governed by absolute value and difference of the excitatory and inhibitory time constants.

2 Models

In the following section, we provide a detailed analysis of two minimal models for periodicity identification on the basis of excitatory–inhibitory interplay. The models are ‘minimal’ in that they feature two neurons or neuron populations at most and only two synapses, one inhibitory and one excitatory (Fig. 1).

Analogous to the considerations in the introduction, the first model consists of two neurons or neuron populations (Friedel et al. 2007). If the input neuron (population) fires a spike, it is fed into two distinct pathways leading to the output neuron (population). One pathway will project onto the output neuron via an excitatory synapse, the other, delayed pathway via an inhibitory synapse. In a biological realization the delayed pathway will consist of at least one reliable interneuron. Certain combinations of delay, inhibitory and excitatory time constants, as well as the strength of the synapses will lead to maximal firing rates for different frequencies. We call this model the *feedforward model*.

The second model consists of a single neuron (or, again, a neuron population) that receives an input signal via an excitatory synapse. If the neuron spikes, the output spike will be fed into a pathway (again biologically realized by an interneuron) that projects back to the neuron itself with a particular delay. The spike will result in an *inhibitory* PSP characterized by its strength and a time constant different from the excitatory one. Such a setting leads, as we will see in the following sections, to a maximal firing rate for one specific frequency. A set of neurons, each with different time constants and coupling strengths should then act as a frequency analyzer. We call this model the *recurrent model*.

2.1 Detailed description of the feedforward model

The feedforward model features an input neuron population of Poisson neurons (van Hemmen 2001). That is, we assume the firing of the input neurons to be a statistical process, an *inhomogeneous* Poisson process. Such a Poisson process is defined by three properties. First, the probability of finding a spike between t and $t + \Delta t$ is $\lambda(t) \Delta t$, so $\lambda(t)$ is the time-dependent firing probability density or rate function. Second, the probability of finding two or more spikes there is $o(\Delta t)$, which means that we ignore their occurrence for small Δt . Third, a Poisson process has independent increments, i.e., events in disjoint intervals are independent.

The Poisson input neurons are driven externally by s_{in} and form a simple input stage for the model, similar to e.g. the auditory nerve. If any of the input neurons fires, its spike is fed into two pathways, one excitatory and one inhibitory, to a output neuron population, Poisson neurons again. The excitatory spike reaches the output neurons directly, the inhibitory spike is delayed by Δ due to interneurons. We note that in principle the delay Δ could be negative, that is, the excitatory spike could be delayed more than the inhibitory one by excitatory interneurons. Since we want to keep the setup simple and in biological systems excitatory signals usually are converted into inhibitory signals by means of inhibitory interneurons, delayed inhibition is a reasonable assumption. The connection to every output neuron population is therefore described by a specific combination of inhibitory time constant τ_{inh} , delay Δ and inhibitory coupling strength J_{inh} on the one hand and excitatory time constant τ_{exc} and excitatory coupling strength J_{exc} on the other hand.

If a spike is emitted at time $t = t_0$ by any input neuron it leads to two postsynaptic responses ε in the output neuron, for which we will take weighted α -functions (Gerstner and Kistler 2002),

$$\varepsilon_{exc} = J_{exc} \frac{t - t_0}{\tau_{exc}^2} e^{-(t-t_0)/\tau_{exc}} \theta(t - t_0) \tag{1}$$

and

$$\varepsilon_{inh} = J_{inh} \frac{t - t_0 - \Delta}{\tau_{inh}^2} e^{-(t-t_0-\Delta)/\tau_{inh}} \theta(t - t_0 - \Delta). \tag{2}$$

Here J is the synaptic weight, positive for excitatory and negative for inhibitory synapses, t_0 the spiking time of the presynaptic neuron, τ determines the width of the α -function, and Δ is the delay of the inhibition. θ denotes the Heaviside step function [$\theta(t) = 0$ if $t < 0$, $\theta(t) = 1$ if $t \geq 0$].

2.2 Detailed description of the recurrent model

The recurrent model consists of Poisson output neurons (van Hemmen 2001) that are driven by the continuous input function s_{in} convoluted with the excitatory postsynaptic current. All neurons feature a recurrent connection that feeds output spikes back into the neuron. The recurrent connection is characterized by a specific combination of inhibitory time constant τ_{inh} , delay Δ , and inhibitory coupling strength J_{inh} . Again, inhibitory and excitatory currents are described by α -functions of the form (1) and (2).

3 Mathematical discussion of the models

We are now going to mathematically discuss the behavior of the two types of periodicity detectors.

3.1 Feedforward model

We mimic a realistic, usually half-wave rectified periodic signal by a shifted cosine similar to the (positive) envelope of an AM signal. As a consequence of the properties of a Poisson neuron (van Hemmen 2001), this input function then describes the inhomogeneous firing probability density λ_{in} of the input neuron,

$$s_{in}(t) = \frac{A}{2} [1 - \cos(2f\pi t)] = \lambda_{in}(t). \tag{3}$$

The total response ε of one specific output neuron to the input neuron activity is given by [referring to (1) and (2)]

$$\varepsilon_{total} = \varepsilon_{exc} + \varepsilon_{inh}. \tag{4}$$

The firing probability density λ_{out} of the output neurons is then given by

$$\lambda_{out}(t) = \int_{-\infty}^{\infty} ds s_{in}(s) \varepsilon_{total}(t - s). \tag{5}$$

Equation (5) can be evaluated exactly for the given input function (3) with result

$$\lambda_{\text{out}}(t) = \frac{1}{2} J_{\text{exc}} \left[\frac{(1+4\zeta_{\text{exc}}^2)^2 + (-1+4\zeta_{\text{exc}}^2) \cos(2f\pi t)}{(1+4\zeta_{\text{exc}}^2)^2} - \frac{-4\zeta_{\text{exc}} \sin(2f\pi t)}{(1+4\zeta_{\text{exc}}^2)^2} \right] + \frac{1}{2} J_{\text{inh}} \left[\frac{(1+4\zeta_{\text{inh}}^2)^2 + (-1+4\zeta_{\text{inh}}^2) \cos[2f\pi(t-\Delta)]}{(1+4\zeta_{\text{inh}}^2)^2} - \frac{4\zeta_{\text{inh}} \sin[2f\pi(t-\Delta)]}{(1+4\zeta_{\text{inh}}^2)^2} \right] \tag{6}$$

where we assumed $A = 1$ and $\zeta_j = f\pi\tau_j$ for $\tau_j = \tau_{\text{exc}}$ and τ_{inh} , respectively. The symmetry between excitation and delayed inhibition is obvious.

In order to analyze (6), it is desirable to reduce the number of free parameters. We therefore set $J_{\text{exc}} = 1$ in the following. Furthermore, it is easy to see that (6) is of the form $\lambda_{\text{max}}(J_{\text{inh}}; \Delta; \tau_{\text{exc}}; \tau_{\text{inh}}; f) \times \cos(2f\pi t + \phi)$, ϕ being a phase-shift of no further interest. It is thus sufficient to consider the amplitude λ_{max} to obtain an understanding of the system:

$$\lambda_{\text{max}} = \frac{1}{2} + \frac{J_{\text{inh}}}{2} + \left\{ \frac{1}{2(1+4\zeta_{\text{exc}}^2)^2(1+4\zeta_{\text{inh}}^2)^2} \times \left[(J_{\text{inh}} + 4J_{\text{inh}}\zeta_{\text{exc}}^2)^2 + (1+4\zeta_{\text{inh}}^2)^2 + 2J_{\text{inh}}(1+16\zeta_{\text{exc}}^2\zeta_{\text{inh}}^2 - 4\zeta_{\text{exc}}^2 + 16\zeta_{\text{exc}}\zeta_{\text{inh}} - 4\zeta_{\text{inh}}^2) \cos(2f\pi\Delta) + 8J_{\text{inh}}(\zeta_{\text{exc}} - \zeta_{\text{inh}})(1+4\zeta_{\text{exc}}\zeta_{\text{inh}}) \sin(2f\pi\Delta) \right] \right\}^{\frac{1}{2}} \tag{7}$$

Next, we want to get rid of J_{inh} as a free parameter. For an optimal performance of our model the maximum of the response should be a clear peak. We can minimize λ_{max} at the boundary of the range of frequencies we are interested in; that is, positive frequencies. If λ_{max} is minimal at the left and at the right border of the frequency range under consideration, the peak, somewhere in between these two limits, should be easy to distinguish. At $f = 1$ Hz, λ_{max} is minimal for an inhibitory coupling strength J_{inh} of -1 to -0.99 , depending on the parameters chosen. This is true for the complete range of accessed parameters; that is Δ , τ_{exc} , and τ_{inh} taking any value from 1 ms to 10 ms each. At the same time, the limiting value of (7) for $f \rightarrow \infty$ is $(1 + J_{\text{inh}})/2$. The optimal inhibitory coupling J_{inh} is therefore -1 , the same absolute value as the excitatory coupling. This is called *balanced inhibition*.

In what follows, we will take the delay Δ to be 2 ms. This assumption is equivalent to our concept of constructing a ‘minimal’ model since, in order to turn an excitatory signal inhibitory, we need at least one interneuron. Two milliseconds are a reasonable time for a signal passing one neuron.

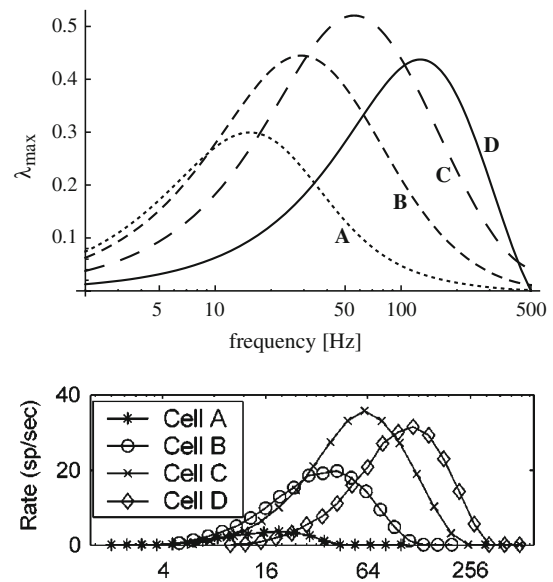


Fig. 2 Frequency detection by excitatory–inhibitory networks. *Top* time-invariant amplitude λ_{max} of the firing probability density against frequency of the input signal s_{in} . Four sets of parameters are shown, each resulting in a maximum of the amplitude at different frequencies. Characteristics of the solutions match numerical results from Nelson and Carney (2004); cf. *bottom panel*. The parameters except J_{inh} were taken from Nelson and Carney (2004): A($\tau_{\text{exc}}; \tau_{\text{inh}}$) = (5 ms; 10 ms), B(2 ms; 6 ms), C(1 ms; 3 ms), D(1 ms; 1 ms); $\Delta = 2$ ms; $J_{\text{inh}} = -1$. *Bottom* absolute rate modulation transfer function of the SFIE model (Nelson and Carney 2004), rate versus frequency [Hz]. Four different model cells in the inferior colliculus have been simulated, every cell responding maximally to a certain modulation frequency of the signal. The match of analytical and numerical results for identical parameters is surprising since the SFIE model (Nelson and Carney 2004) is much more complicated than our setup

At the end of this section we will discuss the influence of the delay and its variation on the behavior of model.

Figure 2, top panel, illustrates the behavior of the solution (7) for four different parameter sets. We see that the solutions have a clear maximum for one *specific* frequency ranging from about 14 Hz (solution A) to approximately 140 Hz (solution D), depending on the combination of time constants τ_{exc} and τ_{inh} . Before analyzing (6) further, it is interesting to compare its behavior with numerical simulations published before (Nelson and Carney 2004). In the latter, time constants as well as delay between excitation and inhibition we have used have led to almost identical results (see Fig. 2, bottom panel). It is noteworthy that, motivated by physiological findings, the setup of the model of Nelson and Carney (2004) is much more complicated than here: two subsequent stages of delayed inhibition and excitation with different coupling strengths featuring three cell populations (auditory nerve, cochlear nucleus, and inferior colliculus) and four synapses lead to quantitatively the same results regarding frequency selectivity.

Ideally, a maximum that is to be discerned clearly should have a big amplitude (in this respect, cell A in the bottom

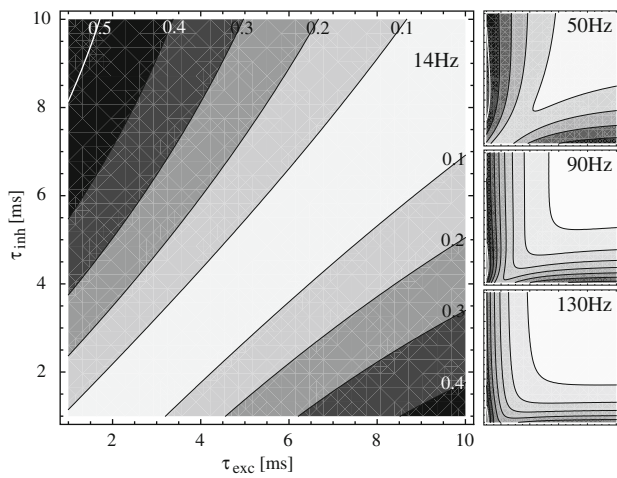


Fig. 3 Amplitude of the response of the feedforward model for low and high-frequency signals with a fixed delay as a function of excitatory and inhibitory time constant. *Black* stands for a large, *white* for a small amplitude. *Big* low-frequency stimuli (here: 14 Hz) lead to two clearly separated areas of maximal response. The response is maximal for a large difference of τ_{exc} and τ_{inh} , and a larger inhibitory time constant results in a higher amplitude (~ 0.5 versus ~ 0.4 in the case of larger excitatory time constant). *Right, top to bottom* (units same as on the *left*): increasing frequency of the stimulus (here: 50, 90, and 130 Hz) leads to a merge of the two areas of maximal response and a decreasing amplitude. The amplitude is maximal when either excitatory or inhibitory time constant is very small. Here $\Delta = 2 \text{ ms}$, $J_{inh} = -1$

panel of Fig. 2 would be a bad example). As a consequence we are interested in the regions of our solution where the amplitude λ_{max} is maximal. Since an analytical solution is not feasible we will revert to a graphical approach.

Figure 3 shows the amplitude of the solution (7) for different time constants and frequencies. For low frequencies we can discern two distinct regions of maximal amplitude: amplitude is maximal when inhibitory and excitatory time constants have a maximal difference (dark areas). In the figure, the amplitude is minimal for $\tau_{inh} = \tau_{exc} + 0.5\Delta$ (bright area), but this relation only holds if Δ is small compared to the time scale of the frequency under consideration. As the frequency increases (right side of Fig. 3, top to bottom), the two regions of maximal amplitude move towards the origin and merge. The overall amplitude shrinks but is still largest for one of the time constants being very small. At 130 Hz, finally, the amplitude maximum is reached at combinations of very small inhibitory with even smaller excitatory time constants.

The response magnitude’s dependence upon excitatory and inhibitory time constant as shown in Fig. 3 does not, however, elucidate how the frequency with maximal response amplitude depends on the combination of excitatory and inhibitory time constant (as well as delay). Since the derivative of λ_{max} (7) with respect to inhibitory and excitatory time constants is not tractable analytically, we have to stick to a graphical solution once more. Figure 4 depicts the depen-

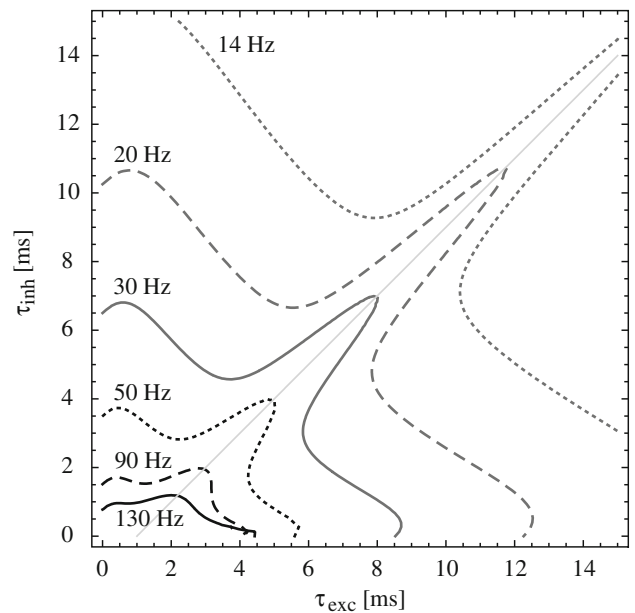


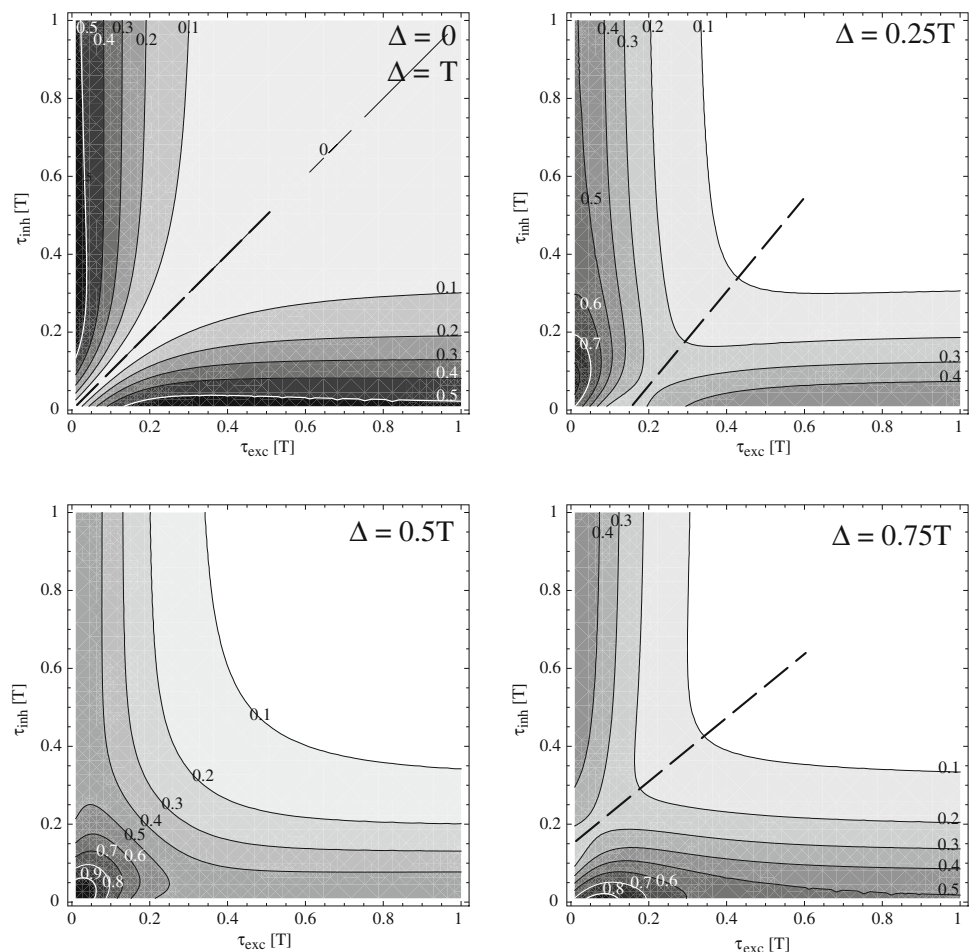
Fig. 4 Contours of the maximal response amplitude in the τ_{inh} - τ_{exc} -plane for different signal frequencies with fixed delay. *Black solid, dashed, and dotted line, gray solid, dashed, and dotted line*: amplitude maxima for 130, 90, 50, 30, 20, and 14 Hz; *thin gray line*: $\tau_{inh} = \tau_{exc} + 0.5\Delta$. As the frequency increases, the maximal amplitude appears at smaller time constants. We note that the performance of the model can only be estimated in combination with the absolute amplitude (cf. Fig. 3). Here $\Delta = 2 \text{ ms}$, $J_{inh} = -1$

dence of the maximum of (6) upon excitatory and inhibitory time constants. Generally, lower time constants lead to a maximum for higher frequencies. Lower frequencies can be accessed by larger time constants, leading to no strict cut-off in the low-frequency range. The delay breaks the symmetry of the solution and results in an ‘anomaly’ along the line $\tau_{inh} = \tau_{exc} + 0.5\Delta$ if $\Delta \ll 1/f$. Since the amplitude of the solution is minimal along this axis, useful maxima lie at small values of either the excitatory or inhibitory time constant. In principle every combination of a small excitatory with a larger inhibitory time constant has an equivalent combination of small inhibitory with larger excitatory time constant, but the discrimination ability for high frequencies is poorer (see maximum for 90 and 130 Hz in Fig. 4). In addition, combinations of small excitatory with larger inhibitory time constants lead to higher amplitudes, so that our original idea of filtering and subtracting different frequencies with help of different time constants seems suggestive.

The considerations above are, however, only valid if the assumption of Δ being much smaller than $T = 1/f$ holds. If Δ is varied independently of f the landscape of the solution changes, as Fig. 5 illustrates, drastically.

Figure 5 shows the amplitude λ_{max} as a function of dimensionless time constants τ' and delay Δ' . We define dimensionless units x' as $x' = x/T$. For integer multiples of the cycle periods T of the signal the amplitude behaves very

Fig. 5 Influence of the delay on the amplitude in dimensionless units. Amplitude of the solution to (7) as a function of dimensionless excitatory and inhibitory time constant in cycle periods T of the signal. *Upper left* in case of no delay or the delay matching exactly one period of the signal frequency, the solution is completely symmetric relative to excitatory and inhibitory time constants. *Upper right* increasing delay shifts the axis of the minimum to larger excitatory time constants and the maximum to the origin. *Lower left* a delay of $T/2$ leads to a maximal response for minimal excitatory and inhibitory time constants; that is, δ -functions as PSPs. *Lower right* the axis of the minimum reappears at further increase of the delay, this time at larger inhibitory time constants. Since, we are interested in low frequencies and delays of limited length, only the regime displayed in the upper panel is relevant. $J_{\text{inh}} = -1$



similar to Fig. 3, big panel, viz., two distinct areas of maximal amplitude separated by a diagonal of minimal response. The reason is that a delay of 2 ms is small compared to the cycle period of 14 Hz, ~ 70 ms. Increasing the delay Δ (Fig. 5: to $0.25T$) shifts the axis of minimum response to the right; that is, to larger excitatory time constants. At the same time the maximum moves towards smaller inhibitory time constants. The very same behavior occurs when signal frequency is increased but the delay is kept constant. The increase of frequency from 14 Hz to 50, 90, and 130 Hz at a constant delay of 2 ms in Fig. 3 corresponds to an increase of the delay from $0.028T$ to 0.1 , 0.18 , and $0.26T$ in the current setting. At a delay corresponding to half the cycle period of the signal, symmetry is restored and a single maximum exists at $(\tau_{\text{exc}}; \tau_{\text{inh}}) = (0; 0)$; that is, the PSPs behave like δ - instead of α -functions. Since at this particular delay the inhibitory signal operates in the valley of the excitatory signal, a minimal excitatory–inhibitory interference leads to a maximal response. The minimal interference is provided by δ -functions as PSPs. At a further increase of the delay the maximum wanders towards larger excitatory time constants and a second maximum appears for small excitatory and large inhibitory time constants. For $\Delta = T$, the contour of the

amplitude is finally symmetric again, featuring two clearly separated areas of maximal response.

Two considerations restrict our interest to the regime shown in the upper half of Fig. 5. First, in various animals, most neurons that are sensitive to amplitude modulation are responding maximally to frequencies between 30 and 100 Hz. Second, the initial motivation for a model of neuronal frequency identification by means of inhibition has been the lack of evidence for delay lines with $\Delta > 10$ ms in biological systems, so only “short” delays are of interest to us. A delay of 4 ms, which is a value well within the range of physiological constraints, corresponds to $0.5T$ at 125 Hz. In order to obtain a maximal response to amplitude modulated stimuli in this frequency range, it therefore makes sense to combine small excitatory with larger inhibitory time constants.

The delay can also be varied so as to allow a broader range of frequencies. A very short delay of $\Delta = 0.3$ ms pushes the upper limit of about 140 Hz for a Δ of 2 ms to about 500 Hz (result not shown). Longer delays extend the accessible frequency range to lower frequencies. Changing the delay from 2 ms to a Δ of 15 ms, for example, lowers the preferred frequency for $(\tau_{\text{exc}}; \tau_{\text{inh}}) = (1; 15.5)$ from 14 to 10 Hz (result not shown).

With a given delay we can take the excitatory time constant to be a very small value (e.g. 1 ms) and vary the inhibitory time constant in order to control the preferred frequency of our model (cf. Fig. 4). We thus arrive at a neuronal band-pass filter characterized by the biologically plausible variation of a single parameter, the inhibitory time constant.

The analytical calculations above have been verified by numerical simulations (data not shown). There we have used a population of Poisson input neurons and LIF output neurons. The outcome matched our results very closely. This was to be expected, since Eq. (5) describes not only the firing probability density for Poisson neurons but also holds for the expectation value of an input current to LIF neurons (Friedel et al. 2007). Interestingly, the phase locking of the output spikes has been increased by the model even further than in a comparable setting (Friedel et al. 2007).

3.2 Recurrent model

The idea of a neuronal band-pass filter we have developed in the last section can be compressed into an even simpler setup. One single population of neurons suffices if we use a recurrent inhibitory connection; see the bottom panel of Fig. 1. In order to cope with the feedback, we will consider Poisson neurons for our analytic calculations.

For sufficient neuronal activity (Friedel et al. 2007) we can describe the rate function λ of a single Poisson neuron or neuron population projecting back to itself with a particular delay time Δ by the integral equation

$$\begin{aligned} \lambda(t) &= J_{\text{exc}} \int_{-\infty}^{\infty} ds g_{\text{exc}}(s) s_{\text{in}}(t-s) \\ &\quad + J_{\text{inh}} \int_{-\infty}^{\infty} ds g_{\text{inh}}(s; \Delta) \lambda(t-s) \\ &= J_{\text{exc}}(g_{\text{exc}} \star s_{\text{in}})(t) + J_{\text{inh}}(g_{\text{inh}} \star \lambda)(t). \end{aligned} \tag{8}$$

The rate function consists of the sum of the external input s_{in} and the delayed inhibitory input from the recurrent loop, both ‘smeared out’ by the kernel g_{exc} and g_{inh} , respectively. The feedback strength is given by J_{inh} and we choose g to be α -functions as in (1) and (2) so as to ensure causality and obtain unit weights.

To solve Eq. (8) we change to Fourier space where convolutions are ordinary products. The Fourier-transformed version of (8) reads

$$\Lambda(\omega) = J_{\text{exc}} G_{\text{exc}}(\omega) S_{\text{in}}(\omega) + J_{\text{inh}} G_{\text{inh}}(\omega) \Lambda(\omega), \tag{9}$$

where the Fourier transform of each input term is denoted by a capital letter. The solution is thus given by

$$\Lambda = \frac{J_{\text{exc}} G_{\text{exc}}}{1 - J_{\text{inh}} G_{\text{inh}}} S_{\text{in}} \tag{10}$$

and can be transformed back into a function of time by taking its inverse Fourier transform.

In a way similar to the last section, we mimic a half-wave rectified signal by a shifted cosine function

$$s_{\text{in}}(t) = \frac{1}{2} [B - \cos(2f\pi t)] \tag{11}$$

where B denotes the shift of the cosine along the y-axis. This is a necessary precaution in order to avoid a negative rate function. We obtain a solution that is, just as in the feedforward model, of the form

$$\lambda(t) = \lambda_{\text{max}}(B; J_{\text{exc}}; J_{\text{inh}}; \Delta; \tau_{\text{exc}}; \tau_{\text{inh}}; f) \times \cos(2f\pi t + \phi). \tag{12}$$

As before, ϕ is a phase-shift of no further interest. For any finite solution we can find an B that can shift the solution to positive values and prevent a negative rate function. Since this shift does not affect the solution otherwise, we can as well forego the shift; that is, set $B = 0$ for the sake of convenience. We now turn to the time-invariant amplitude λ_{max} that is of interest for a characterization of the system,

$$\lambda_{\text{max}} = \frac{J_{\text{exc}} (4f^2\pi^2\tau_{\text{inh}}^2 + 1)}{\sqrt{2} \sqrt{\Upsilon^2 + \Omega^2}} \tag{13}$$

where

$$\begin{aligned} \Upsilon &= \sqrt{2} J_{\text{inh}} \left(-1 + 4\zeta_{\text{exc}}^2 \right) + 2\sqrt{\pi} \\ &\quad \times \left\{ \left[1 + 16\zeta_{\text{exc}}^2 \zeta_{\text{inh}}^2 - 4 \left(\zeta_{\text{exc}}^2 \right. \right. \right. \\ &\quad \left. \left. \left. + 4\zeta_{\text{exc}} \zeta_{\text{inh}} + \zeta_{\text{inh}}^2 \right) \right] \cos(2f\pi \Delta) \right. \\ &\quad \left. + 4(\zeta_{\text{exc}} + \zeta_{\text{inh}}) (-1 + 4\zeta_{\text{exc}} \zeta_{\text{inh}}) \sin(2f\pi \Delta) \right\} \end{aligned} \tag{14}$$

and

$$\begin{aligned} \Omega &= -4J_{\text{inh}} \sqrt{2} \zeta_{\text{exc}} - 2\sqrt{\pi} \\ &\quad \times \left\{ \left[1 + 16\zeta_{\text{exc}}^2 \zeta_{\text{inh}}^2 - 4 \left(\zeta_{\text{exc}}^2 \right. \right. \right. \\ &\quad \left. \left. \left. + 4\zeta_{\text{exc}} \zeta_{\text{inh}} + \zeta_{\text{exc}}^2 \right) \right] \sin(2f\pi \Delta) \right. \\ &\quad \left. + 4(\zeta_{\text{exc}} + \zeta_{\text{inh}}) (-1 + 4\zeta_{\text{exc}} \zeta_{\text{inh}}) \cos(2f\pi \Delta) \right\} \end{aligned} \tag{15}$$

with $\zeta_j = f\pi\tau_j$ for $\tau_j = \tau_{\text{exc}}$ and τ_{inh} . In order to reduce the number of parameters we set $J_{\text{exc}} = 1$.

Figure 6 illustrates the performance of the recurrent model. Parameter sets that are identical to the ones we have used in the example for the feedforward model (Fig. 2) lead to a very similar behavior, viz., maximal response at virtually identical frequencies. The peaks are, however, less clear since for low frequencies the amplitude does not drop as in the feedforward model. In addition, the overall amplitudes are lower.

For a quantitative understanding of the recurrent model, we proceed as in the last section and change to dimension-

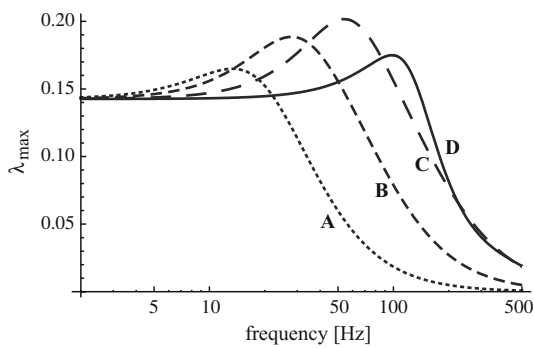


Fig. 6 Frequency detection of the recurrent excitatory–inhibitory network for balanced inhibition in the form of the time-invariant amplitude λ_{\max} of the rate function against the frequency of the input signal s_{in} . The parameter sets are identical to those of Fig. 2 and lead to a maximal response for virtually identical frequencies. The quality of the peaks is low as compared to the feedforward model. A smaller overall amplitude and a relatively high amplitude for low frequencies deteriorates the recurrent network performance. Parameter values are A(τ_{exc} ; τ_{inh}) = (5 ms; 10 ms), B(2 ms; 6 ms), C(1 ms; 3 ms), D(1 ms; 1 ms); $\Delta = 2 \text{ ms}$; $J_{\text{inh}} = -1$

less units. We derive the inhibitory coupling strength J_{\max} for which the dimensionless version of (13) is maximal,

$$J_{\max} = \sqrt{2\pi} \left[(1 - \zeta_{\text{inh}}^2) \cos(2f\pi \Delta) - \zeta_{\text{inh}} \sin(2f\pi \Delta) \right] \tag{16}$$

By combining this inhibitory coupling strength with the dimensionless version of (13) we arrive at a λ_{\max} that is dependent only on the excitatory and inhibitory time constant as well as the delay (in dimensionless units),

$$\lambda_{\max} = \frac{1}{\sqrt{2\pi}} \times \frac{1 + \zeta_{\text{inh}}^2}{(1 + \zeta_{\text{exc}}^2) [2\zeta_{\text{inh}} \cos(\zeta_{\Delta}) + (1 - \zeta_{\text{inh}}^2) \sin(\zeta_{\Delta})]} \tag{17}$$

where $\zeta_{\Delta} = 2f\pi \Delta$. Obviously the excitatory time constant does not characterize the band-pass response of the model but simply scales the amplitude; we will not discuss this parameter in the following.

We can now easily derive a constraint for the relation between inhibitory time constant $\zeta_{\text{inh}} = f\pi \tau_{\text{inh}}$ and delay $\zeta_{\Delta} = f\pi \Delta$: Equation (17) is maximal if

$$\zeta_{\Delta} = \arctan\left(\frac{2\zeta_{\text{inh}}}{\zeta_{\text{inh}}^2 - 1}\right) + n\pi \tag{18}$$

with $n = 0$ if $\zeta_{\text{inh}} > 1$ and $n = 1$ if $\zeta_{\text{inh}} < 1$. For the inhibitory time constant approaching zero, that is, δ - instead of α -functions as PSPs, (18) reduces to $\zeta_{\Delta} = \pi$ or, in dimensional units,

$$\Delta = \frac{1}{2f} = 0.5 T, \tag{19}$$

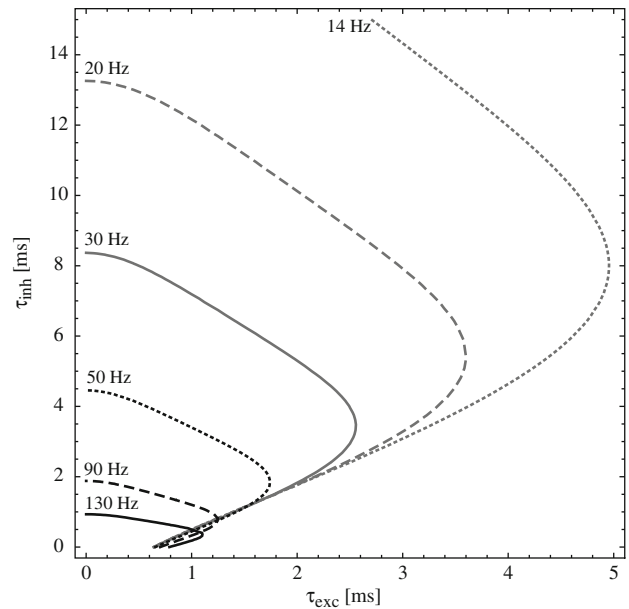


Fig. 7 Contours of the maximal response amplitude in the $\tau_{\text{inh}}\text{-}\tau_{\text{exc}}$ -plane for different signal frequencies with fixed delay for the recurrent model. *Black solid, dashed, and dotted line, gray solid, dashed, and dotted line*: amplitude maxima for 130, 90, 50, 30, 20, and 14 Hz. As the frequency increases, the maximal amplitude appears at smaller time constants. We note that the performance of the model can only be estimated in combination with the absolute amplitude; largest amplitudes are obtained for small excitatory time constants (data not shown). In contrast to the feedforward model, all maxima that are characteristic for a given frequency feature inhibitory time constants that are larger than the excitatory ones. Here, $\Delta = 2 \text{ ms}$, $J_{\text{inh}} = -1$

just as in the feedforward model where the amplitude is maximal for $(\tau_{\text{exc}}; \tau_{\text{inh}}) = (0; 0)$ if the delay is $0.5 T$.

Equation (18) could be interpreted as if an arbitrary short delay could be compensated by an appropriate inhibitory time constant. This is not the case since, as a consequence of (16), such an arbitrary short delay would require a *very* large inhibitory coupling (e.g., a delay of $\Delta = 0.05 T$ would result in $\tau_{\text{inh}} = T$ and $J_{\text{inh}} = -101$). But how far can we get with a realistic inhibitory coupling?

From Fig. 6 we see that restricting the inhibitory strength to a balanced inhibition ($J_{\text{inh}} = -1$) as in the feedforward model still gives reasonable results. What is, however, the relation between parameter set and preferred frequency, the frequency for which the response of the model is maximal? Analytic insight is easy in dimensionless units but hard to transfer into dimensional units, so we will stick to a graphical approach as in the last section.

The relation between excitatory time constant, inhibitory time constant, and preferred frequency is shown in Fig. 7. As in the feedforward model, lower (inhibitory) time constants lead to a maximum for higher frequencies. However, contrary to the feedforward model, there is no symmetry between combinations of large excitatory with small inhibitory and combinations of large inhibitory with small excit-

atory time constants. All maxima that are characteristic to a given frequency feature inhibitory time constants that are larger than the excitatory ones. Since the amplitude of the solution is maximal for small excitatory time constants (data not shown), it makes sense to choose the excitatory time constant as small as possible. The result is a system where—given delay and inhibitory strength fixed—the frequency response can again be tuned over one order of magnitude by the inhibitory time constant alone.

4 Discussion

As we have seen, a simple feedforward model can identify frequencies in the range of approximately ten to several hundred Hertz relying on biologically plausible parameters only, viz., short delays and balanced inhibition. The model works best for a very short, fixed excitatory time constant. Given a specific delay the preferred frequency of the model where the response is maximal can be varied by tuning the inhibitory time constant. Alternatively, the inhibitory time constant can be taken to be short and the model can be tuned by the excitatory time constant. A recurrent setup shows a behavior very similar to the feedforward model and can identify frequencies in the same range. The amplitude peaks, however, are shallow when compared to the response maxima in the feedforward model. Furthermore, in contrast to the feedforward model, a short excitatory time constant is necessary for the model to work. Again, the model can be tuned by choosing the appropriate inhibitory time constant.

Interestingly, the characteristics of the neuronal band-pass filter at hand are quite different from the initial conception we have formulated in the introduction. The naive picture of simply subtracting the envelopes of two low-pass-filtered signals does not explain the characteristics of the system. If the neuronal band-pass filter would follow such a naive picture and we had defined the cut-off frequency as the frequency where the response of the system is half of the maximal response, the preferred frequency would be given by $f_{\text{pref}} = 1/(4\pi^2 \tau_{\text{exc}} \tau_{\text{inh}})^{1/2}$. This would lead to hyperbolic-like curves in Fig. 4. Obviously an in-depth mathematical description is crucial to an accurate analysis of the system.

Although motivated by our intention to create a ‘minimal model’, the delay of 2 ms chosen in the current calculations may seem arbitrary. Appearances are deceiving, however, as experimental results of inhibition being delayed by 2.4 (Wehr and Zador 2003) and 2 ms (Las et al. 2005) have been found in cortex. In the auditory brainstem, one could expect even shorter delays as 0.6 ms for the inhibition (Wickesberg 1996). Thinking of the influence a short delay has on the preferred frequency of our model, these short delays fit the concept of the auditory brainstem dealing with higher frequency signal periodicity than the cortex. In fact, sensitivity for amplitude modulations up to 1,000 Hz has been reported in the

experimental literature (Joris et al. 2004). However, neurons sensitive to modulation frequencies >300 Hz are few and far between, while the majority of the neurons is confined to the range of 30–100 Hz. This finding is valid for the auditory brainstem of various animals (Krishna and Semple 2000; Langner and Schreiner 1988; Rees and Møller 1983, 1987; Rees and Palmer 1989) so that, from a conceptual point of view, most of the AM sensitivity of neurons can be explained by our model.

Quite surprisingly, balanced inhibition turns out to be the optimal choice for the inhibitory coupling strength. This is of interest since, as stated in the introduction, BI has been observed at several examples of processing sensory information but its function remained unclear. Our findings suggest that a role in the processing of signal periodicity such as amplitude modulations and/or the processing of vibratory signals would be feasible. The findings of single whisker deflections causing a sequence of excitation and balanced inhibition in the rat barrel cortex (Highley and Contreras 2006) and BI changing the chopping frequency in chopper neurons in the very same animal (Paolini et al. 2005) fit here nicely. The idea of BI acting as a kind of gate or filter between cortical areas (Highley and Contreras 2006) agrees with our present results in that the frequency range of our model covers the β (13–30 Hz) and γ (30–100 Hz) oscillations that are believed to play a role in the communication between different parts of the brain and in attention, a related topic. Furthermore, BI is locked to noise envelopes in the cat auditory cortex and locking is suppressed by low-level tones (Las et al. 2005). This can be taken as a hint towards BI playing a role in the attentional framework.

Acknowledgments The authors thank Paul Friedel and Laurel H. Carney for helpful comments. M.B. and J.L.v.H. were supported by the BCCN, Munich.

References

- Anderson JS, Carandini M, Ferster D (2000) Orientation tuning of input conductance, excitation, and inhibition in cat primary visual cortex. *J Neurophysiol* 84:909–926
- Barth F (1998) The vibrational sense of spiders. In: Hoy RR, Popper AN, Fay RR (eds) *Comparative hearing: insects*, chap. 7. Springer, New York pp 228–278
- Bendor D, Wang X (2005) The neuronal representation of pitch in primate auditory cortex. *Nature* 436:1161–1165
- Bleckmann H, Barth F (1984) Sensory ecology of a semi-aquatic spider *Dolomedes triton* II. The release of predatory behavior by water surface waves. *Behav Ecol Sociobiol* 14:303–312
- Bregman A (1990) *Auditory scene analysis*. MIT Press, Cambridge
- Cherry EC (1953) Some experiments on the recognition of speech, with one and with two ears. *J Acoust Soc Am* 25(5):975–979
- Coombs S, Görner P, Münz H (eds) (1989) *The mechanosensory lateral line: neurobiology and evolution*. Springer, New York
- Elepfandt A (1984) Localization of water surface waves with the lateral line system in the clawed toad (*Xenopus laevis* daudin). In: Varjú

- D, Schnitzler H (eds) *Localization and orientation in biology and engineering*. Springer, New York, pp 63–65
- Friedel P, Bürck M, van Hemmen JL (2007) Neuronal identification of acoustic signal periodicity. *Biol Cybern* 97:247–260
- Gerstner W, Kistler W (2002) *Spiking neuron models*. Cambridge University Press, Cambridge
- Grothe B (1994) Interaction of excitation and inhibition in processing of pure tone and amplitude-modulated stimuli in the medial superior olive of the mustached bat. *J Neurophysiol* 71:706–721
- Highley MJ, Contreras D (2006) Balanced excitation and inhibition determine spike timing during frequency adaptation. *J Neurosci* 26(2):448–457
- Izhikevich EM (2001) Resonate-and-fire neurons. *Neural Netw* 14: 883–894
- Joris PX, Schreiner CE, Rees A (2004) Neural processing of amplitude-modulated sounds. *Physiol Rev* 84:541–577
- Kalmijn A (1988) Hydrodynamic and acoustic field detection. In: Atema J, Fay R, Popper A, Tavolga W (eds) *Sensory biology of aquatic animals*, chap. 4. Springer, New York, pp 83–130
- Käse R., Bleckmann H (1987) Prey localization by surface wave ray-tracing: fish track bugs like oceanographers track storms. *Experientia* 43:290–293
- Krishna B, Semple M (2000) Auditory temporal processing: response to sinusoidally amplitude-modulated tones in the inferior colliculus. *J Neurophysiol* 84:255–273
- Langner G (1992) Periodicity coding in the auditory system. *Hear Res* 60:115–142
- Langner G, Schreiner C (1988) Periodicity coding in the inferior colliculus of the cat. I. Neuronal mechanisms. *J Neurophysiol* 60:1799–1822
- Large EW, Crawford JD (2002) Auditory temporal computation: interval selectivity based on post-inhibitory rebound. *J Comput Neurosci* 13:125–142
- Las L, Stern EA, Nelken I (2005) Representation of tone in fluctuating maskers in the ascending auditory system. *J Neurosci* 25(6): 1503–1513
- Licklider J (1951) A duplex theory of pitch perception. *Experientia* 7:128–134
- Meddis R, O'Mard L (2006) Virtual pitch in a computational physiological model. *J Acoust Soc. Am.* 120(6):3861–3869
- Monier C, Chavane F, Baudot P, Graham LJ, Frégnac Y (2003) Orientation and direction selectivity of synaptic inputs in visual cortical neurons: a diversity of combinations produces spike tuning. *Neuron* 37:663–680
- Nelken I, Rotman Y, Bar Yosef O (1999) Responses of auditory-cortex neurons to structural features of natural sounds. *Nature* 397: 154–157
- Nelson PC, Carney LH (2004) A phenomenological model of peripheral and central neural responses to amplitude-modulated tones. *J Acoust Soc Am* 116(4):2173–2186
- Okun M, Lampl I (2008) Instantaneous correlation of excitation and inhibition during ongoing and sensory-evoked activities. *Nat Neurosci* 11(5):535–537
- Paolini AG, Clarey JC, Needham K, Clark GM (2005) Balanced inhibition and excitation underlies spike firing regularity in ventral cochlear nucleus chopper neurons. *Eur J Neurosci* 21:1236–1248
- Rees A, Møller A (1983) Responses of neurons in the inferior colliculus of the rat to AM and FM tones. *Hear Res* 10:301–330
- Rees A, Møller A (1987) Stimulus properties influencing the responses of inferior colliculus neurons to amplitude-modulated sounds. *Hear Res* 27:129–143
- Rees A, Palmer A (1989) Neuronal responses to amplitude-modulated and pure-tone stimuli in the guinea pig inferior colliculus, and their modification by broadband noise. *J Acoust Soc Am* 85:1978–1994
- Schreiner C, Langner G (1988) Periodicity coding in the inferior colliculus of the cat. II. Topographical organization. *J Neurophysiol* 60:1823–1840
- Shannon R, Zeng FG, Kamath V, Wygonski J, Ekelid M (1995) Speech recognition with primarily temporal cues. *Science* 270:303–304
- Speck-Hergenröder J, Barth F (1987) Tuning of vibration sensitive neurons in the central nervous system of a wandering spider, *Cupiennius salei* Keys. *J Comp Physiol A* 160:467–475
- van Hemmen JL (2001) Theory of synaptic plasticity. In: Moss F, Gielen S (eds) *Handbook of biological physics, neuro-informatics, neural modelling*, vol 4. Elsevier, Amsterdam, pp 771–823
- Wehr M, Zador AM (2003) Balanced inhibition underlies tuning and sharpens spike timing in auditory cortex. *Nature* 426:442–446
- Wickesberg RE (1996) Rapid inhibition in the cochlear nuclear complex of the chinchilla. *J Acoust Soc Am* 100(3):1691–1702
- Yost W (1994) *Fundamentals of Hearing: an introduction*, 3rd edn. Academic, San Diego
- Zhang LI, Tan AYY, Schreiner CE, Merzenich MM (2003) Topography and synaptic shaping of direction selectivity in primary auditory cortex. *Nature* 424(10):201–205